RSC Advances

PAPER

View Article Online
View Journal | View Issue

Cite this: *RSC Adv.*, 2019, **9**, 21451

Study of thermal stability of p-type skutterudites $DD_{0.7}Fe_3CoSb_{12}$ by Knudsen effusion mass spectrometry

František Zelenka,[ab] Pavel Brož,*[ab] Jan Vřešťál,[ab] Jiří Buršík,[c] Gerda Rogl,[de] Andriy Grytsiv[de] and Peter Rogl[de]

Received 29th May 2019
Accepted 1st July 2019

DOI: 10.1039/c9ra04056k

rsc.li/rsc-advances

The temperature and phase stability of p-type skutterudites, $DD_{0.7}Fe_3CoSb_{12}$, manufactured *via* various preparation techniques, all exhibiting a high *ZT*-level, have been studied by means of thermal analysis and Knudsen effusion mass spectrometry. The results from phase transformation measurements and characteristics of the evaporation of antimony, as the volatile element, supported by microstructure observations and by diffusion profiles are summarized and discussed in view of a full understanding of the degradation processes and knowledge of the long term operation stability of the bulk and nano-structured thermoelectrics studied. It was found out that the antimony evaporation is a complex diffusion kinetic process resulting in a stable Sb level dependent on the preparation route. The studied p-type skutterudites, $DD_{0.7}Fe_3CoSb_{12}$, have proven their long term stability in thermoelectric devices at a maximum operation temperature of 600 °C. Complementary data on the structural, physical and mechanical properties of the materials are presented as well.

1 Introduction

Thermoelectric materials have gained increased interest for their ability to motionlessly exploit waste heat (renewable energy) and convert it to electricity. The research in the field of new prospective bulk and nano-structured thermoelectrics is, therefore, of great importance for materials engineering in the automotive and aerospace industry, electronics and other areas. Improvement of thermoelectric materials and production processes concerns their thermoelectric properties, their thermodynamic and phase equilibria and also their long term thermal stability, which strongly depends on the content of volatile constituents as the current advanced materials contain elements like Cd, Zn, Sb, Sr and others. These elements can evaporate under operational conditions, leading to structure changes and to a negative influence of the thermoelectric properties. In this work thermal and phase stability of bulk and nanostructured p-type $DD_{0.7}Fe_3CoSb_{12}$ skutterudites prepared by various procedures including ball milling, hot and cold pressing and high pressure torsion were studied by a combination of differential thermal analysis (DTA) and Knudsen effusion mass spectrometry (KEMS). The measurements of the evaporation characteristics of antimony by the KEMS method, which comprises the main part of the work, were complemented by measurement of the diffusion profiles. The data were subsequently used for evaluation of the diffusion kinetics of the Sb evaporation and for determination of the long term thermal stability of the materials.

2 Skutterudites

Skutterudites present us with tantalizing potential applications in thermoelectrics because of their unique structure.[1–5] Skutterudites are compounds with a body centered cubic crystal structure, space group $Im\bar{3}$,[6] and the simplest compounds *i.e.* unfilled skutterudites, have the formula TX_3 (T is a transition element of the VIII group, *e.g.* Fe, Co, Ni… and X is a pnictogen atom, *e.g.* Sb). Electropositive elements E (E is a rare earth, an actinoid, an alkaline-earth, or an alkaline metal) and electronegative elements such as iodine and others[7] may fill the icosahedral voids, formed by tilted octahedra, in the so called filled skutterudites with the chemical formula $E_yT_4X_{12}$, where y is the filling fraction. Due to the unusually low energy vibrational modes of the filler atoms, called 'rattlers', in the oversized cages, the physics of filled skutterudites is essentially governed by the interplay of filler ions and their host structure.[8–14]

The efficiency of advanced thermoelectric technology is determined by the dimensionless figure of merit, $ZT = S^2T/\rho\lambda$

[a]*Masaryk University, Faculty of Science, Department of Chemistry, Kotlářská 2, 61137, Brno, Czech Republic. E-mail: broz@chemi.muni.cz*

[b]*Masaryk University, Central European Institute of Technology, CEITEC, Kamenice 753/5, 62500, Brno, Czech Republic*

[c]*Institute of Physics of Materials, Czech Academy of Sciences, Žižkova 22, 61662, Brno, Czech Republic*

[d]*Institute of Materials Chemistry, University of Vienna, Währingerstraße 42, A-1090 Vienna, Austria*

[e]*Christian Doppler Laboratory for Thermoelectricity, Vienna, Austria*

where S is the Seebeck coefficient, which is proportional to a voltage ΔV generated by a thermal gradient ΔT ($\Delta V/\Delta T$), T is the absolute temperature, ρ is the electrical resistivity and λ the thermal conductivity, the latter being the sum of the electronic conductivity, λ_e, and the lattice thermal conductivity, λ_{ph} ($\lambda = \lambda_e + \lambda_{ph}$). Reducing λ_{ph} is an important issue to achieve a high ZT. In this work, didymium, DD, consisting of Pr (4.76 mass%) and Nd (95.24 mass%), was used as natural double filler. Pr and Nd have a relative large atomic mass in respect to a small ionic radius providing conditions for rattling of these atoms in the icosahedral voids thereby reducing significantly the thermal conductivity *via* enhanced phonon scattering. The introduction of structural disorder *via* T-metal substitution (Fe/Co) further reduces λ_{ph} (*via* so-called alloy scattering of phonons) and consequently enhances ZT.[15–28] Ball milling (BM) or high energy ball milling (HBM) is employed to produce small particle sizes in order to additionally increase the thermoelectric performance *via* nano-structuring.[29] The "top down methods" like mechanical milling (BM, HBM) followed by hot pressing (HP) are reasonable ways to prepare materials with a crystallite size of the order of several 100 nm and crystal imperfections (*e.g.* dislocation densities of about 10^{12} m^{-2}). With these methods nano-structured multifilled p- and n-type skutterudites have reached remarkable high ZT values ($ZT > 1.4$).

Furthermore Severe Plastic Deformation (SPD) with High Pressure Torsion (HPT), as one of its major representatives, can achieve materials with ultra fine grains in the sub-micrometer or even nanometer range. With this method an extremely large plastic strain under a significantly high hydrostatic pressure is imposed on a sample without any essential change of the sample's geometry, which leads to (i) ultra fine grained structures and (ii) an enhanced formation of lattice defects – vacancies and particularly of dislocations (for details see ref. 28, 30–32). After HPT the lattice defects and grain boundaries reduce the lattice thermal conductivity substantially *via* phonon scattering and thus were found to enhance ZT at least by 20%.[33]

3 Experimental techniques

3.1. Preparation of p-type skutterudites $DD_yFe_3CoSb_{12}$

p-type skutterudites with the nominal composition $DD_{0.7}Fe_3CoSb_{12}$ were prepared from a master alloy Fe_3CoSb_{12} *via* an optimized melting reaction technique from stoichiometric amounts of high purity elements (Fe, 99.5%, wire, Co, 99.9%, powder < 150 micron, Sb, 99.95%, crystals) by mixing, sealing into evacuated quartz tubes, melting at 950 °C followed by air quenching (details are given in ref. 22, 24, 25 and 29). Then the stoichiometric amount of DD (from Treibacher Industries AG, 99.9%) was added. The samples were then sealed under vacuum into quartz tubes, quickly heated to 600 °C, then slowly heated to 720 °C (2 °C min^{-1}) and after a fast rise of the temperature (5 °C min^{-1}), melted at 950 °C and air quenched. The reguli were ground in the glove box to obtain particles < 50 μm, followed by BM (for details of ball-milling conditions see ref. 28) in Ar-filled tungsten carbide vessels (Fritsch planetary mill Pulverisette 4) and hot-pressed, HP, (FCT uniaxial hot-press HP W 200/250 2200-200-KS, Ar, 700 °C, 56 MPa, 30 min). After determination of the composition by EPMA this sample is labeled as $DD_{0.7}Fe_{3.1}Co_{0.9}Sb_{12}$-BM-HP. Additionally HPT was performed with an equipment from W. Klement, Austria: the sample was processed with 4 GPa and one revolution at 400 °C (further on referred to as HPT). For all details of HPT processing of skutterudites the reader is referred to ref. 29–31. Accordingly this sample is labeled as $DD_{0.7}Fe_{3.1}Co_{0.9}Sb_{12}$-BM-HP-HPT.

Furthermore two p-type skutterudite samples were prepared from commercially produced powders from Treibacher Industries AG (TIAG). For one sample ($DD_{0.7}Fe_3CoSb_{12}$-HP) the powder was hot pressed under the same conditions as described above without BM (labelled as $DD_{0.7}Fe_3CoSb_{12}$-HP (TIAG)). For the other sample (labelled as $DD_{0.7}Fe_3CoSb_{12}$-CP-HPT (TIAG)) the original powder was cold pressed (CP) followed by HPT processing at 400 °C under nitrogen (to avoid oxidation) applying 4 GPa and 1 revolution (for details see ref. 33).

A surplus of 3 mass% Sb was added in order to compensate losses in the preparation. In the hot pressing step most of this antimony was squeezed out again and only minor amounts remained at the grain boundaries.

3.2. Study of thermal and phase stability

The study of thermal and phase stability of the materials prepared was performed by means of DTA and KEMS on a Netzsch STA 409 CD/3/403/5/G apparatus, a specially-adapted type of the commercial STA 409 CD-QMS 403/5 Skimmer Coupling Instrument.[34,35]

3.2.1 DTA measurements. Three heating and cooling cycles at a heating and cooling rate of 5 °C min^{-1} were performed during the DTA to exactly specify phase transformations in the material. The alloy $DD_{0.7}Fe_{3.1}Co_{0.9}Sb_{12}$-BM-HP (prepared by common techniques and available in relatively sufficient amount from all the alloys) was chosen for the measurement. In order to prevent Sb evaporation and its potential negative influence on the measured data, the samples were sealed in evacuated quartz ampoules having the same shape like the original alumina crucibles, as discussed in ref. 35. Small pieces with the total weight of approximately 0.5 g were used for every measurement. Argon (purity of 99.9999) at the flow rate of 70 ml min^{-1} was used as carrier gas.

3.2.2 KEMS measurements. Evaporation characteristics of Sb *via* KEMS measurements for the alloy $DD_{0.7}Fe_{3.1}Co_{0.9}Sb_{12}$-BM-HP were investigated in the temperature interval of 530–625 °C; at first for shorter times to gain preliminary information on the stability of the material. Detailed measurements of all alloys at temperatures 530, 560 and 590 °C were consequently performed until limiting values of ion current intensities and hence limiting values of vapour pressure of Sb were achieved, in order to exactly specify the long time thermal stability. The samples $DD_{0.7}Fe_{3.1}Co_{0.9}Sb_{12}$-BM-HP and $DD_{0.7}Fe_3CoSb_{12}$-HP (TIAG) were studied at the first two temperatures only due to their limited amount. Samples in form of tablets having approximately 400 mg for the preliminary measurement and 100–250 mg for the long time measurements were placed in the Knudsen cell and measured. Measurement of pure Sb was performed after the measurement of each sample and the data

were used for evaluation of the evaporation processes of Sb from the investigated material. Pieces of Sb having approximately 400 mg were used for the measurement. Monitoring of monomer ions of the Sb isotopes generated at ionization energy of 35 eV was preferred due to their largest response from all measured oligomers, as found during the instrument calibration by measurement of the heats of sublimation of selected elements[34] and as also used in our recent study of the thermal stability of primary $CoSb_3$ skutterudite.[36]

3.3. Measurement of diffusion profiles

Depth profiles of element distribution were measured on samples after thermal exposure at 530, 560 and 590 °C using a Tescan LYRA 3XMU SEM×FIB scanning electron microscope (SEM) working at acceleration voltage of 20 kV and equipped with an X-Max 80 Oxford Instruments detector for energy dispersive X-ray analysis (EDX). Bulk samples were mechanically polished to remove several tens of micrometres of the surface layer and final stages of polishing were done very gently using a Buehler VibroMet vibratory polisher to produce a sample edge as sharp as possible for near-surface profile measurements. Regarding the sample edge curvature and the interaction volume of EDX analyses, the depth of the region influenced could be measured with an uncertainty of about 1 μm.

3.4. Determination of the structure; physical and mechanical properties measurements

Details of measurements (X-ray intensity data, density, crystallite size, electrical resistivity, Seebeck coefficient, thermal conductivity, hardness) are summarized in our previous articles on the subject.[28–31]

4 Results and discussion

4.1. Physical, structural and mechanical properties

Whereas the crystallite size for $DD_{0.7}Fe_{3.1}Co_{0.9}Sb_{12}$-BM-HP (153 nm) is reduced to 54 nm after HPT, the dislocation density is enhanced for the HPT processed sample $DD_{0.7}Fe_{3.1}Co_{0.9}Sb_{12}$-BM-HP-HPT from 2.8×10^{13} m^{-2} to 2.6×10^{14} m^{-2}. These changes are reflected in the physical properties (see below). The relative density (d_{rel} = 98.9%) was higher for $DD_{0.7}Fe_{3.1}Co_{0.9}Sb_{12}$-BM-HP than for $DD_{0.7}Fe_{3.1}Co_{0.9}Sb_{12}$-BM-HP-HPT ($d_{rel}$ = 97.5%), because of the introduction of fine micro cracks during HPT. For $DD_{0.7}Fe_{3.1}Co_{0.9}Sb_{12}$-BM-HP a ZT = 1.2 at 725 K was reported, which is one of the highest values for a p-type skutterudite. The HPT processed sample, due to smaller grains and higher dislocation density, $DD_{0.7}Fe_{3.1}Co_{0.9}Sb_{12}$-BM-HP-HPT had a higher electrical resistivity, which was overcompensated by a much lower thermal conductivity, especially in the temperature range of about 500–600 K, when the electrical resistivity decreases from a maximum value. This behavior together with a slightly enhanced Seebeck coefficient raises ZT to ZT > 1.4 at 725 K (for details see ref. 28, 30 and 31).

The lattice parameters of $DD_{0.7}Fe_{3.1}Co_{0.9}Sb_{12}$-BM-HP and $DD_{0.7}Fe_{3.1}Co_{0.9}Sb_{12}$-BM-HP-HPT were a = 0.91123(2) nm and a = 0.91128(3) nm, but after the measurement with the Knudsen cell the lattice parameter of $DD_{0.7}Fe_{3.1}Co_{0.9}Sb_{12}$ is slightly smaller: a = 0.91118(2) nm. The Hall–Petch-type relation applies for HPT processed skutterudites: the smaller the crystallite size, the harder the alloy. Regardless of the fact that the higher the density, the harder the material, $DD_{0.7}Fe_{3.1}Co_{0.9}Sb_{12}$-BM-HP has HV 0.1 ∼ 460, whereas $DD_{0.7}Fe_{3.1}Co_{0.9}Sb_{12}$-BM-HP-HPT reveals HV 0.1 > 500 in the center and HV 0.1 > 600 in the rim area, the part of the sample exposed to the highest shear strain during HPT processing (for details see ref. 28, 30 and 31).

$DD_{0.7}Fe_3CoSb_{12}$-HP and $DD_{0.7}Fe_3CoSb_{12}$-CP-HPT follow the trend of $DD_{0.7}Fe_{3.1}Co_{0.9}Sb_{12}$-BM-HP and $DD_{0.7}Fe_{3.1}Co_{0.9}Sb_{12}$-BM-HP-HPT with a smaller grain size and a higher dislocation density, a slightly bigger lattice parameter and a lower relative density for the HPT processed sample (see Table 1; data adopted from ref. 28, 30 and 31).

For convenience to the reader Fig. 1 summarizes the ZT values as a function of temperature and mechanical properties (hardness) *vs.* density of the materials for which the Sb-evaporation has been studied in this work.

4.2. Differential thermal analysis

Information on the phase stability of $DD_{0.7}Fe_3CoSb_{12}$ and respective phase transitions is crucial in the process of preparation and investigation of the thermal stability of the material. DTA yields valuable information for the selection of a maximum temperature up to which the thermal stability can be investigated. The DTA measurement was done on the $DD_{0.7}Fe_{3.1}Co_{0.9}Sb_{12}$-BM-HP alloy as mentioned in Section 3. This alloy prepared by common procedures can be taken as the representative for all the investigated alloys. The first measurement was realized up to 1000 °C in order to gain a complete series of phase transformation temperatures (see Fig. 2a). The second measurement realized up to 700 °C was aimed at a precise identification of the ternary transformation close to the binary eutectic isotherm (liquid ↔ $CoSb_3$ + Sb, see also ref. 36) at about 620 °C, which is a limiting temperature factor for the thermal stability of the $CoSb_3$ skutterudite based thermoelectric materials (see ref. 36). The respective DTA record is shown in Fig. 2b. Samples, before and after the measurements, are shown in Fig. 3. Whilst the complete series of phase transformations led to sample decomposition, it is not the case of the eutectic reaction only. The temperatures of the phase transitions, as identified for the $DD_{0.7}Fe_3CoSb_{12}$ skutterudite, are somewhat different in comparison with those in the binary Co–Sb[36,37] and especially in the ternary Fe–Co–Sb[38] system. As for the Fe–Co–Sb

Table 1 Lattice parameter, a, in nm; crystallite size, cs, in nm; dislocation density, dld, in 10^{14} m^{-2}; relative density, d_{rel}, in %; ZT. Data adopted from ref. 28, 30 and 31

Compound	a	cs	dld	d_{rel}	ZT
$DD_{0.7}Fe_{3.1}Co_{0.9}Sb_{12}$-BM-HP	0.91123(2)	152	0.28	98.7	1.2
$DD_{0.7}Fe_{3.1}Co_{0.9}Sb_{12}$-BM-HP-HPT	0.91128(3)	53	2.6	98.1	1.4
$DD_{0.7}Fe_3CoSb_{12}$-HP (TIAG)	0.91086(4)	76	0.9	99.7	1.1
$DD_{0.7}Fe_3CoSb_{12}$-CP-HPT (TIAG)	0.91126(3)	44	3.6	98.0	1.3

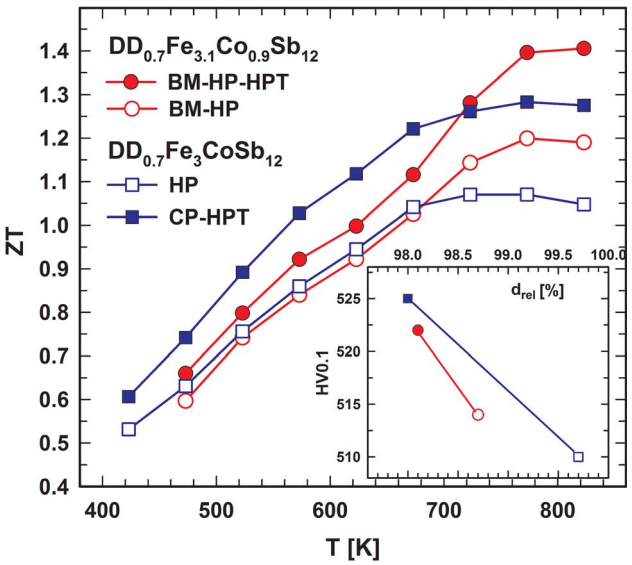

Fig. 1 Summary of figure of merit data *ZT vs.* temperature as well as Vickers hardness *vs.* density for the compounds with various treatments studied in this work.

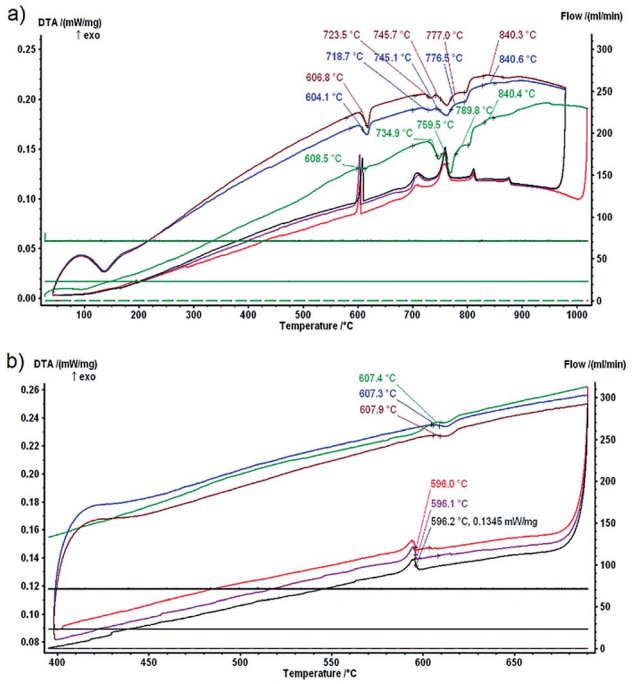

Fig. 2 DTA measurement of the alloy $DD_{0.7}Fe_{3.1}Co_{0.9}Sb_{12}$-BM-HP to (a) 1000 °C and (b) 700 °C at a heating and cooling rate of 5 °C min^{-1} and Ar flow rate of 70 ml min^{-1}. First heating (green line), second heating (blue line) and third heating (brown line) (for interpretation of the references to colour in this figure legend, the reader is referred to the web version of this article).

system, one can notice that the $Co_{1-x}Fe_xSb_3$ skutterudite is only stable for Fe concentrations lower than $x \sim 0.26$ at 580 °C,[38] whereas the DD-filler stabilizes the $DD_{0.7}Fe_3CoSb_{12}$ skutterudite (and even $DDFe_4Sb_{12}$). The phase stability of the $DD_{0.7}Fe_3CoSb_{12}$ skutterudite is mainly governed by Nd, which

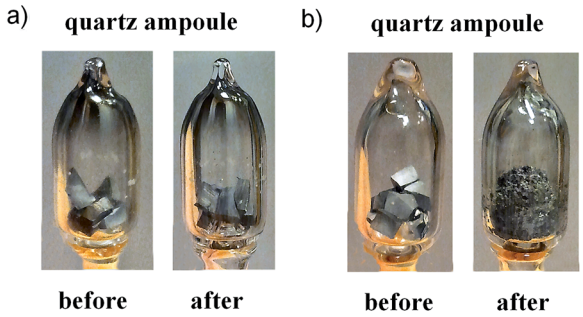

Fig. 3 Quartz ampoule with sample $DD_{0.7}Fe_{3.1}Co_{0.9}Sb_{12}$-BM-HP before and after DTA measurement to (a) 700 and (b) 1000 °C.

constitutes 95.24 mass% of DD. The stabilization effect of Nd for a ternary skutterudite $NdFe_4Sb_{12}$ is already obvious in the Nd–Fe–Sb system.[39–41] However, it should be noted that although single crystal data have shown various degrees of defects in the Nd sublattice ($Nd_{0.832}Fe_4Sb_{12}$,[42] $Nd_{0.73}Fe_4Sb_{12}$ (ref. 43)), phase diagram studies usually display full stoichiometry for $Nd_1Fe_4Sb_{12}$.[39,41] Data from the thermal analysis gained in this work can be used for thermodynamic and phase equilibria studies of quaternary Nd–Fe–Co–Sb or quinary Pr–Nd–Fe–Co–Sb systems, however, the aim of this paper is not a study of phase transformations and phase equilibria in these higher order systems. According to this information and on the basis of our DTA data, the compound $DD_{0.7}Fe_3CoSb_{12}$ should decompose between 720 to 780 °C. This is also consistent with (a) phase diagram calculations by Wang *et al.*[39] indeed revealing a phase decomposition of $NdFe_4Sb_{12}$ at 777 °C, (b) experimental data of Zeng *et al.*[41] and Evers *et al.*,[42] who observed the skutterudite at 500 °C and 600 °C, respectively, as well as (c) experimental data of Nasir *et al.*,[40] which document the non-existence of $Nd_{1-x}Fe_4Sb_{12}$ at 800 °C. The heat effects at high temperatures visible on heating and cooling curves of the DTA record (Fig. 2a) include the decomposition of the $DD_{0.7}Fe_3CoSb_{12}$ skutterudite and phase transformations with other intermetallic phases, originating during cooling, and with liquid phase (see the signals between 800 and 900 °C on the cooling curve).

4.3. Knudsen effusion mass spectrometry

The preliminary effusion measurement, performed on the alloy $DD_{0.7}Fe_{3.1}Co_{0.9}Sb_{12}$-BM-HP in a wide temperature range as a sequence of vapour pressure measurements at various increasing temperatures, showed different sublimation behavior below and above the eutectic temperature of the system, visible as a sudden increase of the ion current intensity above the phase transition temperature about 610 °C on Fig. 4. In comparison with the vapour pressure measurement of pure Sb as the reference material, the results of which are given in ref. 34, performed after the measurement of skutterudite, no obvious linear temperature dependence of the logarithm of the partial pressure of Sb was found. Besides, the measurement of the skutterudite revealed an exponential decrease of the partial pressure of Sb at constant temperatures (see Fig. 4), and as

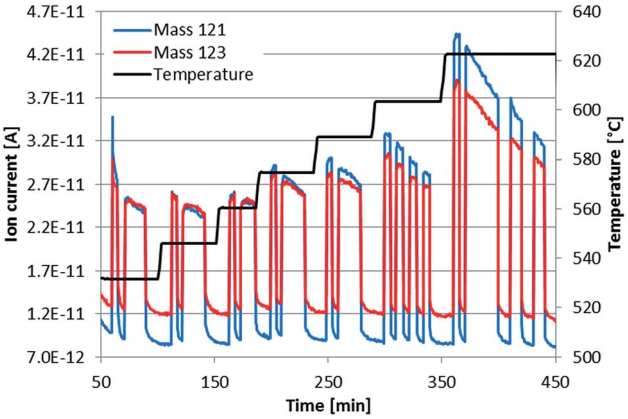

Fig. 4 Vapour pressure measurement of Sb at increasing temperature steps (upper line) in the temperature interval of 530–625 °C for the sample $DD_{0.7}Fe_{3.1}Co_{0.9}Sb_{12}$-BM-HP. Ion current intensities of monomers ^{121}Sb and ^{123}Sb (in the order of decreasing intensity) acquired at an electron energy of 35 eV (background values create the minima). Multiple abrupt drops of ion current correspond to closing the shutter between the Knudsen cell and the ion source, which was done to check the stability of the measured signals and to reduce potential contamination of the ion source by Sb.

expected, falling finally down to limiting values of the partial pressure in infinite time, which indicates a complex diffusion kinetic process and the structure stability of the skutterudite. The exponential decrease of the partial pressure of Sb shows an easy and fast initial release of free or weakly bound Sb from the material, most likely the small amount of surplus free Sb appearing during the preparation of the material, as mentioned in Section 3.1 sample preparation. The limiting values can be assigned to the partial pressure of Sb from the skutterudite $DD_{0.7}Fe_3CoSb_{12}$. For a theoretical description of the exponential behavior, the diffusion equation (eqn (1)) was used

$$y = a_1 e^{(-a_2(x-a_3))+a_4}, \quad (1)$$

where y and x introduce the ion current intensity and time and a_1–a_4 are fitting parameters.

The equation yielded similar limiting values of the vapour pressure of Sb of about 0.5 Pa. These values were taken as preliminary information for subsequent measurements at selected constant temperatures. The subsequent long time measurements led to experimentally determined limiting values of the vapour pressure of Sb (see Fig. 5a–c as an example for alloy $DD_{0.7}Fe_{3.1}Co_{0.9}Sb_{12}$-BM-HP-HPT and Table 2), which were used for the calculation of mass depletion of samples by Sb evaporation. For this purpose the Hertz–Knudsen equation (eqn (2)) was applied,

$$\frac{dn_{Sb}}{dt} = \frac{p_{Sb} A_0 C}{\sqrt{2\pi RTM_{Sb}}}, \quad (2)$$

where n_{Sb} is the number of moles of Sb, t is the time in seconds, p_{Sb} is the partial pressure of antimony, A_0 is the area of the effusion orifice and C is its Clausing factor, R is the molar gas constant, T is the temperature in Kelvin and M_{Sb} is the molar mass of antimony.

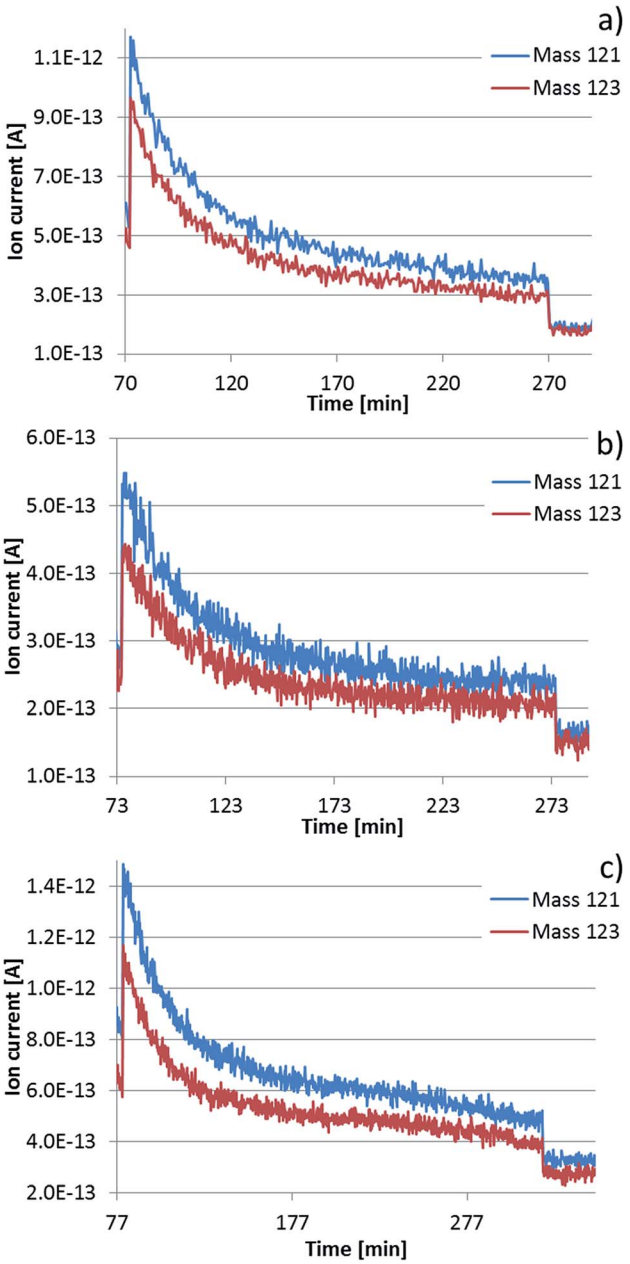

Fig. 5 Vapour pressure measurement of Sb at (a) 530, (b) 560 and (c) 590 °C for the sample $DD_{0.7}Fe_{3.1}Co_{0.9}Sb_{12}$-BM-HP-HPT. Ion current intensities of monomers ^{121}Sb and ^{123}Sb (in the order of decreasing intensity) acquired at an electron energy of 35 eV (minima at the curve ends represent background values).

The calculated values are compared with the measured mass loss (weighed values obtained using a normal analytical balance) in Table 2 and Fig. 6, both recalculated to mass loss per day and relative mass loss per day. As can be seen, a reasonable agreement was obtained. The data are crucial for the evaluation of the time dependent thermal stability of the skutterudites. However, one has to consider that they describe the situation at very low-pressure conditions, which is far from reality because the thermoelectric materials need to be encapsulated under argon reaching normal pressure at maximum operation

Table 2 Vapour pressure of Sb and sample mass loss due to Sb evaporation calculated by Hertz–Knudsen equation (eqn (2)) and measured (weighed) values

Compound	Temperature [°C]	Mass [mg]	Vapour pressure of Sb [Pa]	Loss of mass [mg d^{-1}]		Loss of mass [% d^{-1}]	
				Calculated	Measured	Calculated	Measured
$DD_{0.7}Fe_{3.1}Co_{0.9}Sb_{12}$-BM-HP	531.5	171.3	0.145	5.5	5.8	3.2	3.4
	560.2	191.7	0.236	8.7	7.8	4.6	4.1
$DD_{0.7}Fe_{3.1}Co_{0.9}Sb_{12}$-BM-HP-HPT	531.4	192.9	0.103	3.9	9.6	2.0	5.0
	560.1	159.4	0.200	7.4	7.8	4.6	4.9
	588.7	194.6	0.259	9.4	11.5	4.8	5.9
$DD_{0.7}Fe_3CoSb_{12}$-HP (TIAG)	531.5	254.4	0.097	3.7	1.6	1.4	0.6
	560.1	134.3	0.101	3.7	2.5	2.8	1.9
$DD_{0.7}Fe_3CoSb_{12}$-CP-HPT (TIAG)	531.6	107.8	0.261	9.8	7.2	9.1	6.7
	560.1	128.2	0.341	12.6	12.6	9.8	9.8
	588.8	119.3	0.506	18.4	17.1	15.4	14.3

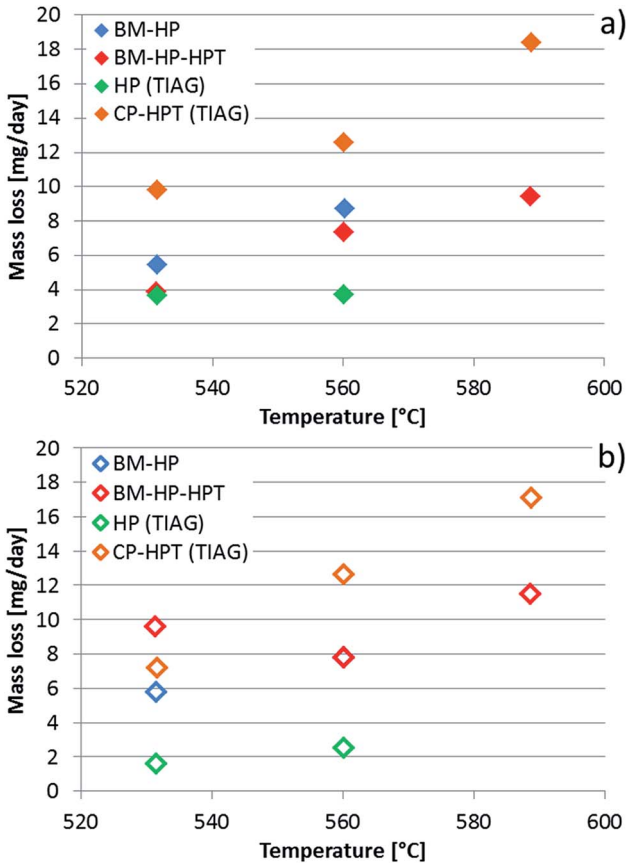

Fig. 6 Plot of sample mass loss from Table 2, (a) calculated and (b) measured values.

temperature. This experiment enables us to do *in situ* monitoring of volatile components, here Sb, and shortens the time for reaching a stable limiting state in comparison with that performed at common operation pressure conditions, requiring very long time periods and not allowing a direct measurement of the volatile species (see ref. 44). It enables us to investigate diffusion kinetic processes and the stability of the skutterudite structure. Fig. 6 clearly shows differences in the process of Sb evaporation from the same $DD_{0.7}Fe_3CoSb_{12}$ skutterudite prepared by various procedures or by their combinations. In all cases the evaporation of Sb increases with increasing temperature in accordance with increasing vapour pressure of Sb. While the highest Sb evaporation was found for the sample prepared by CP and HPT, the lowest one can be attributed to the sample prepared by HP technique. The samples $DD_{0.7}Fe_{3.1}Co_{0.9}Sb_{12}$-BM-HP-HPT and $DD_{0.7}Fe_{3.1}Co_{0.9}Sb_{12}$-BM-HP exhibit similar evaporation characteristics. The different behavior can be explained by the respective preparation procedures. The CP technique does not remove or squeeze out the surplus of Sb present as a densification aid in sample preparation and therefore, the sample contains the biggest amount of free Sb. HPT creates a dense concentration of crystal defects, which can serve as escape way for Sb. The role of BM on the vaporization efficiency cannot be unambiguously defined but the experiments show the material processed by BM reveals higher Sb evaporation than that unprocessed by this technique. The relations are visible from Fig. 6. In addition to these findings, the filled $DD_{0.7}Fe_{3.1}Co_{0.9}Sb_{12}$-BM-HP skutterudite revealed lower Sb vaporization than its unfilled $CoSb_3$ base,[36] prepared by the same procedures, as also already stated in ref. 44. Moreover, a slight increase of the limiting value of the partial pressure of Sb going through a maximum and finally turning back can be seen for the measurement at the highest temperature 590 °C (see Fig. 5c), similarly as already found during the study of thermal stability of the unfilled $CoSb_3$ base,[36] indicating a partial surface decomposition of skutterudite. This was later confirmed by measurement of diffusion profiles (see Section 4.4).

4.4. Diffusion profiles

Diffusion profiles were measured on polished cross-sections as a series of point EDX analyses starting about 1 μm from the sample edge to avoid unassured geometry (Fig. 7a). More severe changes of chemical composition in some samples were accompanied by the creation of a porous multiphase layer; in such cases we rather used a series of EDX analyses from thin rectangular regions parallel to the sample edge (Fig. 7b) to get around local inhomogeneities and obtain averaged depth profiles.

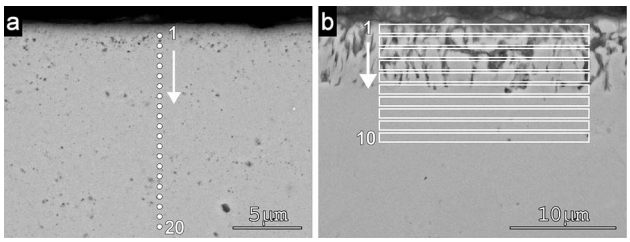

Fig. 7 SEM micrographs, scheme of EDX depth profile measurements for sample $DD_{0.7}Fe_{3.1}Co_{0.9}Sb_{12}$-BM-HP-HPT exposed to 560 °C (a) and $DD_{0.7}Fe_3CoSb_{12}$-CP-HPT (TIAG) exposed to 590 °C (b).

Fig. 8 shows concentration profiles measured on sample $DD_{0.7}Fe_{3.1}Co_{0.9}Sb_{12}$-BM-HP-HPT after exposure to three different temperatures. No clear Sb-depleted zone is observed in the sample exposed at 530 °C, but a zone of 2.5 μm develops at 560 °C and of about 5.5 μm at 590 °C. Other samples show a similar temperature dependence: the Sb-depleted depth is 1.5 μm (530 °C) and 3 μm (560 °C) in sample $DD_{0.7}Fe_3CoSb_{12}$-HP (TIAG) and 1.5 μm (530 °C), 5.5 μm (560 °C) and 7.5 μm (590 °C) in sample $DD_{0.7}Fe_3CoSb_{12}$-CP-HPT (TIAG), respectively.

4.5. Thermal and phase stability

As follows from the results gained, there is a slightly different vaporization behavior of Sb among the materials prepared by various procedures including BM, CP or HP and HPT or their combinations. It can be explained by existence of nano-grains possessing a large surface area (BM and HPT techniques) in comparison with micro-sized particles (without the use of BM and HPT techniques) as well as by existence of structure defects (HPT technique) or by pressing the materials at room (CP) or at elevated (HP) temperatures. Generally, good thermal stability of all studied p-type skutterudites $DD_{0.7}Fe_3CoSb_{12}$ was found.

Besides, G. Rogl *et al.* recently reported on long term stability tests (up to 8880 h) on sample specimens hot pressed from commercially available p- and n-type skutterudite powders (p-type $DD_{0.7}Fe_3CoSb_{12}$ and $(Sm, MM)_{0.2}Co_4Sb_{12}$ (MM = rare earth mischmetal) both from TIAG production 2012).[44] For this study a p- and n-type pair of specimens was placed in the 600 °C hot zone of a silica tube, keeping the cold end at 80 °C. The tubes were sealed at room temperature but were backfilled with argon at a pressure of 300 mbar to reach a pressure of 1 bar at the studied temperature of 600 °C. During the whole test period only slight Sb-losses were observed with a slight decrease of doping levels. Thus the figure of merit ZT_{800K} remained for p-type in the range of 0.9 ± 0.1, but for the n-type material ZT_{800K} slightly decreased from 1.2 to 1.0. Total weight changes were about 0.5 mass% weight gain for the n-type and about 1.2 mass% loss for the p-type material; both weight changes stabilized after ~1000 h.

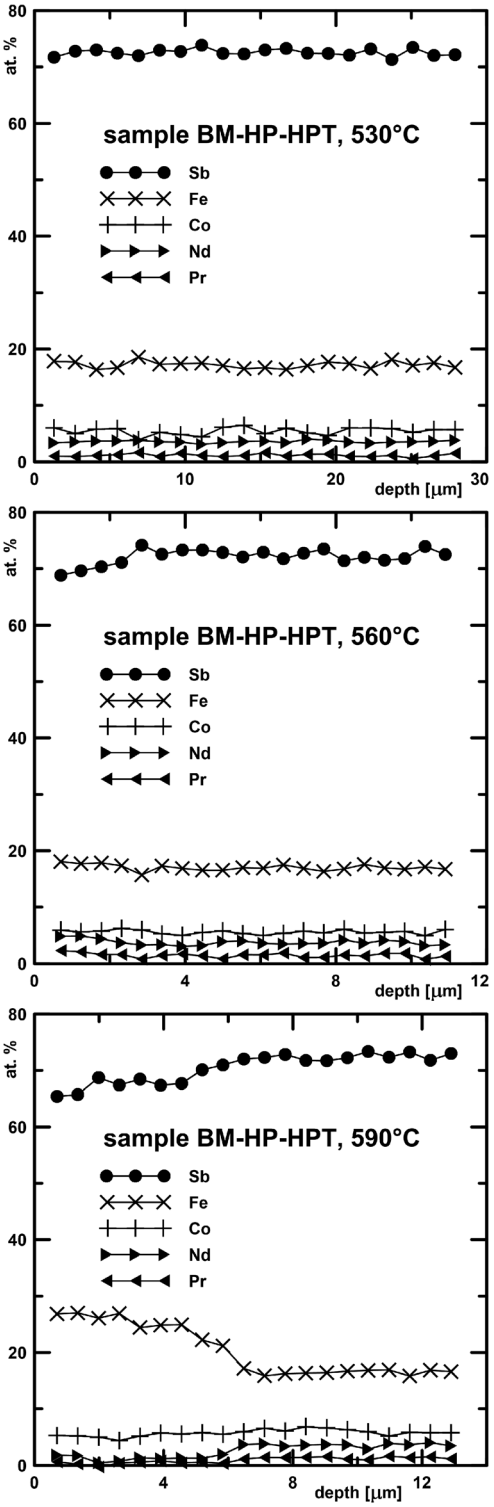

Fig. 8 Depth profiles measured by EDX on sample $DD_{0.7}Fe_{3.1}Co_{0.9}Sb_{12}$-BM-HP-HPT exposed at 530, 560 and 590 °C.

5 Conclusions

Combination of DTA and KEMS was used for the investigation of thermal stability of p-type skutterudites $DD_{0.7}Fe_{\sim3}Co_{\sim1}Sb_{12}$ prepared by BM, CP, HP and HPT procedures or by their combinations. These materials reach a ZT of 1.4 at 600 °C. DTA yielded information on phase transformation temperatures and on the temperature limit for KEMS investigations given by the ternary transformation close to the binary eutectic reaction liquid ↔ $CoSb_3$ + Sb. No linear temperature dependence of

logarithm of partial pressure of Sb was found by KEMS as it was in case of pure Sb, measured as the reference material after every sample measurement. The partial pressure is exponentially reaching a limiting value, which can be assigned to the partial pressure of the skutterudite structure. The Sb evaporation is a complex diffusion kinetic process resulting in a stable state defined by the limiting value, which is dissimilar for the same skutterudite prepared by different procedures or by their combinations. Nevertheless, the differences were found to be small. KEMS is a suitable method for *in situ* monitoring of volatile components and shortens the time for reaching a stable limiting state in comparison with annealing performed at common operation pressure (1 bar) requiring very long time periods and not allowing direct measurement of the volatile species. Concentration of all elements in the studied samples after KEMS measurement is almost constant and X-ray diffraction pattern before and after the KEMS measurement is unchanged, confirming the structure stability of the skutterudite structure.

The studied p-type skutterudites, $DD_{0.7}Fe_3CoSb_{12}$, create confidence in their long term use in thermoelectric devices at a maximum operation temperature of 600 °C.

Conflicts of interest

There are no conflicts to declare.

Acknowledgements

The research reported herein was financially supported by the Czech Science Foundation under the project GA 17-12844S as well as by the project CEITEC 2020 (LQ1601) from the Ministry of Education, Youth and Sports of the Czech Republic under the National Sustainability Programme II. The support of OEAD for the joint bilateral project 2019-CZ/01 is gratefully acknowledged. The authors thank Treibacher Industries AG, TIAG, Austria (Dr Markus Hochenhofer) for supplying the skutterudite powder.

References

1 D. M. Rowe, *Handbook of Thermoelectrics*, CRC Press, Boca Raton, FL, 2006.
2 J. S. Sakamoto, H. Schock, T. Caillat, J. P. Fleurial, R. Maloney, M. Lyle, T. Ruckle, E. Timm and L. Zhang, Skutterudite-based thermoelectric technology for waste heat recovery: progress towards a 1 kW generator, *Sci. Adv. Mater.*, 2011, **3**, 621–632.
3 D. M. Rowe, *Modules, Systems, and Applications in Thermoelectrics*, CRC Press, London, 2012.
4 X. Zhou, G. Wang, L. Guo, H. Chi, G. Wang, Q. Zhang, Ch. Chen, T. Thompson, J. Sakamoto, V. P. Dravid, G. Cao and C. Uher, Hierarchically structured TiO_2 for Ba-filled skutterudite with enhanced thermoelectric performance, *J. Mater. Chem. A*, 2014, **2**, 20629–20635.
5 X. Meng, Y. Liu, B. Cui, D. Qin, J. Cao, W. Liu, Z. Liu, W. Cai and J. Sui, High thermoelectric performance of single phase p-type cerium-filled skutterudites by dislocation engineering, *J. Mater. Chem. A*, 2018, **6**, 20128–20137.
6 W. Jeitschko and D. B. Braun, $LaFe_4P_{12}$ filled with $CoAs_3$-type structure and isotypic lanthanoid transition metal polyphosphides, *Acta Crystallogr., Sect. B: Struct. Crystallogr. Cryst. Chem.*, 1977, **33**, 3401–3406.
7 B. Duan, J. Yang, J. R. Salvador, Y. He, B. Zhao, S. Wang, P. Wei, F. S. Ohuchi, W. Zhang, R. P. Hermann, O. Gourdon, S. X. Mao, Y. Cheng, Ch. Wang, J. Liu, P. Zhai, X. Tang, Q. Zhang and J. Yang, Electronegative guests in $CoSb_3$, *Energy Environ. Sci.*, 2016, **9**, 2090–2098.
8 L. Hicks and M. Dresselhaus, Thermoelectric figure of merit of a one-dimensional conductor, *Phys. Rev. B: Condens. Matter Mater. Phys.*, 1993, **47**(24), 16631–16634.
9 G. P. Meisner, D. T. Morelli, S. Hu, J. Yang and C. Uher, Structure and lattice thermal conductivity of fractionally filled skutterudites: Solid solutions of fully filled and unfilled end members, *Phys. Rev. Lett.*, 1998, **80**, 3551–3554.
10 H. Anno, K. Matsubara, Y. Notohara, T. Sakakibara and H. Tashiro, Effects of doping on the transport properties of $CoSb_3$, *J. Appl. Phys.*, 1999, **86**, 3780–3786.
11 R. Venkatasubramanian, E. Siivola, T. Colpitts and B. O'Quinn, Thin-film thermoelectric devices with high room-temperature figures of merit, *Nature*, 2001, **413**, 597–602.
12 L. D. Chen, T. Kawahara, X. F. Tang, T. Goto, T. Hirai, J. S. Dyck, W. Chen and C. Uher, Anomalous barium filling fraction and n-type thermoelectric performance of $Ba_yCo_4Sb_{12}$, *J. Appl. Phys.*, 2001, **90**(4), 1864–1868.
13 G. Chen and A. Shakouri, Heat transfer in nanostructures for solid-state energy conversion, *J. Heat Transfer*, 2002, **124**, 242–252.
14 G. S. Nolas, G. Fowler and J. Yang, Assessing the role of filler atoms on the thermal conductivity of filled skutterudites, *J. Appl. Phys.*, 2006, **100**(4), 43705.
15 B. C. Sales, D. Mandrus and R. K. Williams, Filled skutterudite antimonides: A new class of thermoelectric materials, *Science*, 1996, **22**, 1325–1327.
16 B. C. Sales, D. Mandrus, B. C. Chakoumakos, V. Keppens and J. R. Thompson, Filled skutterudite antimonides: Electron crystals and phonon glasses, *Phys. Rev. B: Condens. Matter Mater. Phys.*, 1997, **56**, 15081.
17 S. Nolas, J. L. Cohn and G. A. Slack, Effect of partial void filling on the lattice thermal conductivity of skutterudites, *Phys. Rev. B: Condens. Matter Mater. Phys.*, 1998, **58**(1), 164–170.
18 V. L. Kuznetsov, L. A. Kutznetsova and D. M. Rowe, Effect of partial void filling on the transport properties of $Nd_xCo_4Sb_{12}$ skutterudites, *J. Phys.: Condens. Matter*, 2003, **15**, 5035–5048.
19 X. Shi, H. Kong, C. P. Li, C. Uher, J. Yang, J. R. Salvador, H. Wang, L. Chen and W. Zhang, Low thermal conductivity and high thermoelectric figure of merit in n-type $Ba_xYb_yCo_4Sb_{12}$ double-filled skutterudites, *Appl. Phys. Lett.*, 2008, **92**, 182101.
20 Y. Z. Pei, J. Yang, L. D. Chen, W. Zhang, J. R. Salvador and J. Yang, Improving thermoelectric performance of caged

compounds through light-element filling, *Appl. Phys. Lett.*, 2009, **95**, 042101.

21 L. Zhang, A. Grytsiv, M. Kerber, P. Rogl, E. Bauer and M. Zehetbauer, Thermoelectric performance of mischmetal skutterudites $Mm_yFe_{4-x}Co_xSb_{12}$ at elevated temperatures, *J. Alloys Compd.*, 2010, **490**, 19–25.

22 G. Rogl, A. Grytsiv, E. Bauer, P. Rogl and M. Zehetbauer, Thermoelectric properties of novel skutterudites with didymium: $DD_y(Fe_{1-x}Co_x)_4Sb_{12}$ and $DD_y(Fe_{1-x}Ni_x)_4Sb_{12}$, *Intermetallics*, 2010, **18**, 57–60.

23 P. F. Qiu, J. Yang, R. H. Liu, X. Shi, X. Y. Huang, G. J. Snyder, W. Zhang and L. D. Chen, High-temperature electrical and thermal transport properties of fully filled skutterudites RFe_4Sb_{12} (R: Ca, Sr, Ba, La, Ce, Pr, Nd, Eu, and Yb), *J. Appl. Phys.*, 2011, **109**, 063713.

24 G. Rogl, A. Grytsiv, P. Rogl, E. Bauer, M. B. Kerber, M. Zehetbauer and S. Puchegger, Multifilled Nanocrystalline p-type didymium - skutterudites with ZT>1, *Intermetallics*, 2010, **18**, 2435–2444.

25 G. Rogl, A. Grytsiv, P. Rogl, E. Bauer and M. Zehetbauer, Enhanced thermoelectric figure of merit in p-type $DD_y(Fe_{1-x}Co_x)_4Sb_{12}$, *Solid State Phenom.*, 2011, **170**, 240–243.

26 C. Zhou, L. Zhang and J. Sakamoto, Thermoelectric Properties of p-type skutterudite nanocomposites, in *Nanoscale Thermoelectrics, lecture Notes in Nanoscale Science and Technology*, ed. X. Wang and Z. M. Wang, Springer Int. Publishing, Switzerland, 2014, pp. 271–302.

27 G. Rogl, A. Grytsiv, P. Rogl, E. Bauer and M. Zehetbauer, A new generation of p-type didymium skutterudites with high ZT, *Intermetallics*, 2011, **19**, 546–555.

28 G. Rogl, A. Grytsiv, P. Rogl, E. Bauer, M. Hochenhofer, R. Anbalagan, R. C. Mallik and E. Schafler, Nanostructuring of p- and n-type skutterudites reaching figures of merit approximately 1.3 and 1.6 respectively, *Acta Mater.*, 2014, **76**, 434–448.

29 L. Zhang, A. Grytsiv, M. Kerber, P. Rogl, E. Bauer, M. J. Zehetbauer, J. Wosik and G. E. Nauer, $MmFe_4Sb_{12}$- and $CoSb_3$-based nano-skutterudites prepared by ball milling: Kinetics of formation and transport properties, *J. Alloys Compd.*, 2009, **481**, 106–115.

30 G. Rogl, P. Rogl, E. Bauer and M. Zehetbauer, Severe Plastic Deformation, a tool to enhance thermoelectric performance, in *Thermoelectric Nanomaterials*, ed. K. Kuomoto and M. Mori, Springer-Verlag, Berlin Heidelberg, 2013, pp. 193–254.

31 G. Rogl, A. Grytsiv, P. Rogl, E. Royanian, E. Bauer, J. Horky, D. Setman, E. Schafler and M. Zehetbauer, Dependence of thermoelectric behaviour on severe plastic deformation parameters: a case study on p-type skutterudite $DD_{0.60}Fe_3CoSb_{12}$, *Acta Mater.*, 2013, **61**, 6778–6789.

32 R. C. Mallik, R. Anbalagan, G. Rogl, E. Royanian, P. Heinrich, E. Bauer, P. Rogl and S. Suwas, Thermoelectric properties of $Fe_{0.2}Co_{3.8}Sb_{12-x}Te_x$ skutterudites, *Acta Mater.*, 2013, **61**, 6698–6711.

33 G. Rogl, A. Grytsiv, R. Anbalagan, J. Bursik, M. Kerber, E. Schafler, M. Zehetbauer, E. Bauer and P. Rogl, Direct SPD-processing to achieve high-ZT skutterudites, *Acta Mater.*, 2018, **159**, 352–363.

34 P. Broz and F. Zelenka, Specially-adapted type of Netzsch STA Instrument as a tool for Knudsen effusion mass spectrometry, *Int. J. Mass Spectrom.*, 2015, **383**, 13–22.

35 P. Brož, F. Zelenka, J. Sopoušek, M. Hejduková, T. Kuběnová and O. Zobač, Thermal analysis and Knudsen effusion mass spectrometry combined in a specially-adapted commercial skimmer coupled instrument (Netzsch), *CALPHAD: Comput. Coupling Phase Diagrams Thermochem.*, 2019, **65**, 86–92.

36 P. Brož, F. Zelenka, Z. Kohoutek, J. Vřešťál, V. Vykoukal, J. Buršík, A. Zemanová, G. Rogl and P. Rogl, Study of thermal stability of $CoSb_3$ skutterudite by Knudsen effusion mass spectrometry, *CALPHAD: Comput. Coupling Phase Diagrams Thermochem.*, 2019, **65**, 1–7.

37 Y. Zhang, Ch. Li, Z. Du and T. Geng, The thermodynamic assessment of the Co-Sb system, *CALPHAD: Comput. Coupling Phase Diagrams Thermochem.*, 2008, **32**, 56–63.

38 L. D. Dudkin and N. K. Abrikosov, Alloying of the semiconductive compound cobalt antimonide $CoSb_3$ (in Russian), *Fiz. Tverd. Tela*, 1959, **1**(1), 142–151.

39 W. Wang, T. Liu, H. Song, S. Xue, W. Zhang, H. Zhang, L. Zhang, Y. Jia, N. Wang, X. Cheng and Ch. Zeng, A Thermodynamic Modeling of the Fe-Nd-Sb System, *Mater. Trans.*, 2016, **57**(2), 103–111.

40 N. Nasir, A. Grytsiv, P. Rogl, D. Kaczorowski and H. S. Effenberger, The system Nd-Fe-Sb: Phase equilibria, crystal structures and physical properties, *Intermetallics*, 2010, **18**, 2361–2376.

41 L. Zeng, P. Qin, L. Nong, J. Zhang and J. Liao, The 773K isothermal section of the Nd-Fe-Sb ternary system, *J. Alloys Compd.*, 2007, **437**, 84–86.

42 C. B. H. Evers, W. Jeitschko, L. Boonk, D. J. Braun, T. Ebel and U. D. Scholz, Rare earth and uranium transition metal pnictides with $LaFe_4P_{12}$ structure, *J. Alloys Compd.*, 1995, **224**, 184–189.

43 E. Bauer, St. Berger, A. Galatanu, Ch. Paul, M. Della Mea, H. Michor, G. Hilscher, A. Grytsiv, P. Rogl, D. Kaczorowski, L. Keller, T. Hermannsdörfer and P. Fischer, Magnetic behaviour of $PrFe_4Sb_{12}$ and $NdFe_4Sb_{12}$ skutterudites, *Phys. Rev. B: Condens. Matter Mater. Phys.*, 2002, **312–313**, 840–842.

44 G. Rogl, A. Grytsiv, E. Bauer and P. Rogl, Thermoelectric Sb-based Skutterudites for medium temperatures - recent advances, in *Advanced Thermoelectrics: Materials, Contacts, Devices and Systems*, ed. Z. Ren, Y. Lan and Q. Zhang, CRC Press, Boca Raton, FL, 2018, pp. 193–230.